7 Subglacial Processes

7.1 INTRODUCTORY CONCEPTS

In a grounded ice sheet, three mechanisms may cause the ice to flow in the direction of decreasing surface elevation. The first mechanism is *internal deformation* as described by Glen's flow law discussed in Chapter 2. The ice deforms under its own weight to relieve the internal stresses. The associated deformational velocity is zero at the glacier base and reaches a maximum at the upper surface (Section 4.2), and is determined by the geometry—through the driving stress—and ice temperature. Typically, these velocities range from less than a few meters per year to a few hundred meters per year and change only slowly over time as the glacier geometry adjusts to mass imbalances. The second flow mechanism, *basal sliding*, becomes important where basal temperatures have reached the pressure melting temperature and subglacial water is present and is responsible for the dynamic behavior exhibited by outlet glaciers of the Greenland and Antarctic ice sheets. The transition from a frozen bed (cold-based glacier) to one that is lubricated by basal water (warm-based glacier) can lead to an increase in discharge by a factor of 10 or more. The third process that may contribute to glacier flow is *deformation of subglacial sediments.* As noted by Clarke (2005), processes that act in the layer extending a few meters above and below the ice-bed interface can have a greater impact on glacier dynamics than processes operating within the ice itself (such as fabric development and temperature changes), yet this layer remains poorly studied and understood.

Many complex theories of glacier sliding have been developed in attempts to derive a sliding relation, linking sliding speed to relevant quantities such as basal drag, bed roughness, water pressure, and many others. However, the range of possible basal substrates (hard rock, deformable sediment, etc.) and interactions between the various basal processes involved has impeded the development of a full theory. Similarly, obtaining suitable field measurements to test proposed sliding relations is hampered by the inaccessibility of the glacier bed. Consequently, most numerical models use an ad hoc sliding relation that is only partially supported by theory or observations.

Weertman (1979) presents an overview of what he termed, "the unsolved general glacier sliding problem." In short, this problem can be stated as, "the determination of the velocity, U, of a small block of ice that is within the glacier and just above the glacier bed" (p. 98). There are many factors that influence the value of this velocity, and these factors cannot be considered separately (although this is often done) because many feedbacks exist. For example, the sliding speed is believed to increase as the thickness of the interstitial water film increases, which leads to more energy being dissipated by the sliding process, allowing more basal ice to be melted, increasing the thickness of the water layer. Also, under the action of sliding, erosion

may occur, which alters the characteristics of the bed surface. An overview of subglacial processes related to glacier dynamics can be found in Clarke (2005), which makes it clear that accounting for all these processes and interactions in a single sliding theory may be an unattainable goal and the search for finding *the* sliding relation an illusory quest. Nevertheless, much can be learned by studying the importance of individual processes, without accounting for all interactions.

Presenting a full overview of all theoretical work and field measurements pertaining to the glacier sliding problem would be a formidable task and probably require an entire book by itself. Therefore, after presenting the classic model for ice sliding over a hard bed, the discussion in the following sections is restricted to some of the main issues, not claiming to be in any way complete and exhaustive.

One of the first attempts at deriving a mathematical model for glacier sliding can be found in Koechlin (1944), who noted that both basal slip and internal deformation contribute to the observed surface velocity. The sliding component causes glacial erosion. By considering balance of forces at the bed of a slab of ice on an incline, he concluded that sliding can occur when the slope of the incline and the ice thickness are sufficiently large to overcome friction or drag, taken to be proportional to the bed roughness (Koechlin, 1944, p. 115). He tested his theory against observations made on a number of mountain glaciers, although he did not actually formulate a sliding law relating the sliding velocity to bed roughness and gravitational driving force.

The first complete theory of glacier sliding was proposed by Weertman (1957a, 1964), who noted that the bed of a glacier is usually irregular, containing many protuberances impeding the flow of ice and preventing sliding by rigid translation. To explain why sliding nevertheless occurs, Weertman proposed two mechanisms, namely, pressure melting (or regelation) and enhanced flow due to stress concentrations around the obstacles. To estimate the velocity associated with each process, Weertman made the assumption that the glacier bed consists of a smooth inclined plane, with cubical protuberances of dimensions L whose centers are separated by a distance λ (Figure 7.1). Otherwise, the bed is assumed to be smooth and unable to support a shear stress. This means that basal resistance must be due to horizontal normal stresses acting against the vertical faces of the cubicals, being compressive

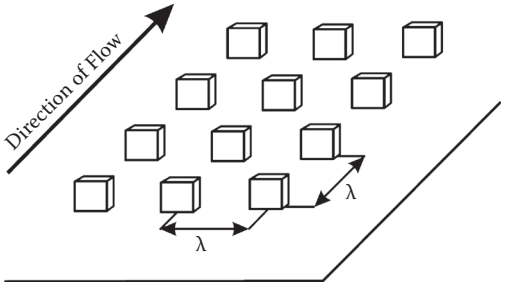

FIGURE 7.1 Idealized model for the glacier bed. Each cube has dimensions L × L × L, and these are separated from each other by a distance λ in both directions. (From Weertman, J., *J. Glaciol.,* 3, 33–38, 1957a. Reprinted from the *Journal of Glaciology* with permission of the International Glaciological Society and the author.)

on the upglacial side and tensile on the downglacial side (so called from drag). This stress difference causes the pressure melting temperature to be lower on the upstream side of the obstacle than on the downstream end. As a result, upstream melting and downstream refreezing occurs, allowing the ice to move around the cube (regelation). The latent heat released by the refreezing is conducted through the obstacle to the upstream side to maintain the temperature difference. Secondly, the stress difference across the obstacles results in enhanced creep of ice around the obstacles.

Consider first the regelation process. In each area of the bed measuring λ by λ, there is one cubic protuberance that provides all basal resistance for this area (frictional traction being zero). If τ_b denotes the average basal drag, then each obstacle must provide a resistive force equal to $\lambda \cdot \lambda \cdot \tau_b$. This resistance is due to an extra compressive stress on the stoss side of the protuberance and an extra tensile stress on the lee side (these normal stresses are in excess of the hydrostatic pressure). From symmetry it follows that the compressive and tensile stresses are equal but of opposite sign. The area upon which these normal forces act is $L \cdot L$ (the side of the obstacle) so that the magnitude of each normal stress is equal to $(\lambda^2 \tau_b / L^2)/2$. This stress difference results in a difference in the pressure melting temperature across the protuberance that is directly proportional to the stress difference. That is

$$\Delta T = \frac{C \tau_b}{R^2}, \tag{7.1}$$

where $R = L/\lambda$ is the bed-roughness parameter and C a constant. If the ice is taken to be at the pressure-melting temperature everywhere, a temperature gradient thus exists across the obstacle, given by (7.1). As a result, heat is conducted across the obstacle in the upglacial direction. Because the distance over which the temperature difference is present is L, the heat flux is given by

$$Q_u = k_b L \, \Delta T, \tag{7.2}$$

where k_b represents the thermal conductivity of the basal material. The assumption is made that there is no flow of heat through the ice. Under steady-state conditions, this upglacial heat flow must be compensated by the release of latent heat on the downglacial side of the obstacle, where meltwater refreezes. The volume of ice that is melted per unit time on the stoss side of the obstacle and refreezes on the lee side is then

$$V = \frac{Q_u}{\rho L_f}, \tag{7.3}$$

with ρ representing the density of glacier ice and L_f the specific latent heat of fusion. The sliding velocity associated with this regelation process follows from the above expressions and is given by

$$U_r = \frac{V}{L^2} = \\ = C_r \frac{\tau_b}{L} R^{-2}. \tag{7.4}$$

Here, C_r represents a constant that incorporates all the material parameters in equations (7.1)–(7.3).

The second process that allows the ice to flow around the basal obstructions is enhanced deformation due to the normal stresses induced by the obstacle. Because the basal resistance arises from these normal stresses and the shear stress parallel to the bed is zero, the constitutive relation (3.48) becomes

$$R_{xx} = 2B\dot{\varepsilon}_{xx}^{1/n}, \tag{7.5}$$

if bridging effects and transverse strain rates may be neglected. As before, the compressive stress on the upglacial face of the obstacle is $(\tau_b R^{-2})/2$ and the strain rate is, from the constitutive relation (7.5),

$$\dot{\varepsilon}_{xx} = -\left(\frac{\tau_b}{4R^2B}\right)^n, \tag{7.6}$$

where the minus sign indicates compression. Making the assumption that this strain rate acts over a distance L upstream of the obstacle, the velocity must decrease over this distance from the sliding value,

$$U_c = \left(\frac{\tau_b}{4R^2B}\right)^n L, \tag{7.7}$$

to zero at the stoss side of the obstacle. Similarly, the tensile strain rate on the lee side results in an increase in velocity from zero to the value given by (7.7) at a distance L downstream of the obstacle.

Comparing the two expressions (7.4) and (7.7) for the sliding velocity associated with both processes shows that, for a given bed roughness (fixed value of R), the pressure-melting mechanism results in increased sliding as the obstacle size decreases, while enhanced creep results in larger sliding around larger obstacles. It may therefore be expected that an intermediate obstacle size exists that offers the most resistance to the flow of the glacier. This size of the controlling obstacle can be found by equating expressions (7.4) and (7.7) and is given by

$$L_c = C_s\left(\frac{\tau_b}{R^2}\right)^{(1-n)/2}, \tag{7.8}$$

where C_s represents a sliding constant incorporating the material parameters and the rate factor. The associated sliding velocity is

$$U_s = C_r\left(\frac{\tau_b}{R^2}\right)^{(1+n)/2}. \tag{7.9}$$

The Weertman theory discussed above was expanded by Nye (1969a, 1970) and Kamb (1970) for arbitrary bed shapes (instead of the rather artificial cubical model).

Both theories are mathematically rigorous and more difficult to understand than the Weertman model but, perhaps surprisingly, yield similar results. The roughness of the bed is described by the spectral power density (Nye) or by a spectral roughness function (Kamb), which is essentially the Fourier series or integral of the basal topography. In both derivations, the roughness is assumed to be small, that is, the difference between the mean bed slope and the actual bed slope is small. Furthermore, both adopt a linear rheology for glacier ice (n = 1). Following Weertman, the basal ice is supposed to be free of debris and separated from the impermeable bed by a thin water film only, so that the form of the lower ice surface is identical to that of the bed. Instead of using a controlling obstacle size, Kamb and Nye introduce the transitional wavelength, λ_t. For basal roughness on scales less than this wavelength, sliding is dominantly by regelation, while for larger roughness scales, the principal sliding mechanism is enhanced creep. The resulting sliding relation is similar to expression (7.9) with n = 1. Kamb (1970) also discusses how the conventional nonlinear constitutive relation can be approximated as a linear relation in the sliding theory. For a "white roughness" (that is, the variance of the basal topography is the same for all wavelengths), he arrives at a similar relation between sliding velocity and basal shear stress as did Weertman. For a "truncated roughness" (in which the short wavelength components are absent), the sliding velocity is proportional to the *n*th power of the basal shear stress.

As pointed out by Lliboutry (1968), a major weakness of the Weertman model is the unrealistically large stress acting on the basal obstructions. The compressive stress on the upglacial side is $(\tau_b R^{-2})/2$. For a basal drag τ_b = 100 kPa and a typical bed roughness R = 0.1, this implies a compressive stress of 5000 kPa and an equally large tensile stress on the downglacier side of the obstacles. Such large tensile stresses would almost certainly lead to basal fracturing or formation of cavities. Moreover, according to equation (7.9), the only controls on the sliding velocity are drag at the glacier base and the roughness of the bed, both of which may be expected to change little over short time spans. However, measurements of surface velocity on alpine glaciers have revealed important short-term fluctuations but no corresponding changes in driving stress. For example, on White Glacier, Iken (1973) observed distinct diurnal variations in the surface velocity during the melt season. After heavy rainfalls, the rate of sliding increased strongly, indicating that variations in subglacial water pressure may be important. Such variations cannot be explained with the Weertman or Nye–Kamb theory. Therefore, the next step must be to investigate sliding when separation between the glacier sole and the bed occurs.

7.2 SLIDING WITH CAVITATION

Cavitation occurs where the basal ice loses contact with the bed, usually on the lee side of a protuberance (Figure 7.2). The first to point out that in addition to the regelation and enhanced creep processes introduced by Weertman (1957a), flow with cavity formation should be considered was Lliboutry (1958a, b). In a series of subsequent papers, he improved and modified the theory for sliding with cavitation (Lliboutry, 1959, 1968, 1979, 1987a, b), and that work has revealed some fundamental aspects that have aided in explaining observed sliding variations on glaciers.

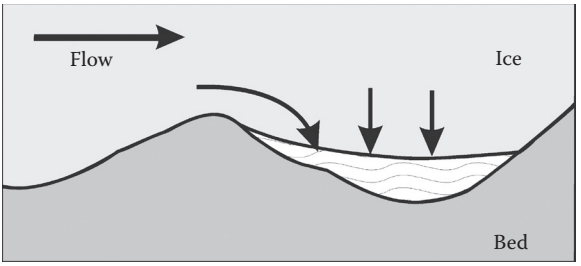

FIGURE 7.2 Formation of subglacial cavities in the lee of topographic irregularities. The smaller arrows indicate closure of the cavity due to advection of ice from upstream and due to vertical downward creep of the ice above. This closure is countered by melting of the cavity roof due to viscous heat dissipation.

The first step is to determine the pressure distribution around a basal obstacle to find an expression for basal drag. To do so, consider first the two mechanisms contributing to the basal resistance. The flow is assumed to be planar, so that from equation (3.20), the net basal resistance is given by

$$\tau_b = R_{xz}(b) - R_{xx}(b)\frac{\partial b}{\partial x}, \tag{7.10}$$

where z = b corresponds to the elevation of the bed. To better understand the physical processes associated with basal drag, consider the components parallel and perpendicular to the bed. Using standard tensor transformation formulas (Section 1.1), the shear stress parallel to the bed is found to be

$$\sigma_{//} = (R_{zz}(b) - R_{xx}(b))\frac{\partial b}{\partial x} + R_{xz}(b), \tag{7.11}$$

while the full stress normal to the bed is given by

$$\sigma_{\perp} = R_{xx}(b)\left(\frac{\partial b}{\partial x}\right)^2 + 2R_{xx}(b)\frac{\partial b}{\partial x} + R_{zz}(b) - \rho g H, \tag{7.12}$$

when higher-order terms may be neglected. The basal resistance can now be written as

$$\tau_b = \sigma_{//} - R_{zz}(b)\frac{\partial b}{\partial x}. \tag{7.13}$$

The first term on the right-hand side represents skin friction and is commonly associated with vertical shear in velocity. If the bed is perfectly lubricated (as in the Weertman and Nye–Kamb theories) this contribution to the basal drag is zero. The second term corresponds to the form drag, which is the resistance due to pressure

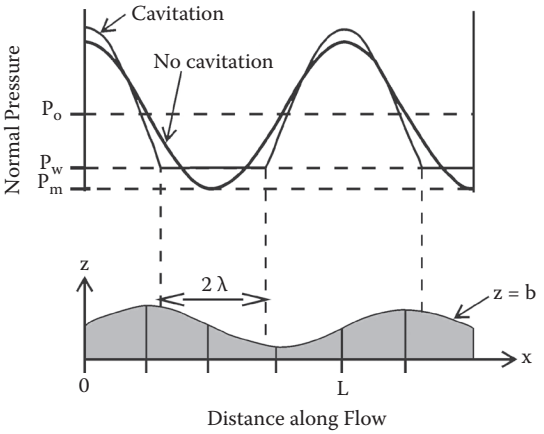

FIGURE 7.3 Bed geometry and normal pressure at the glacier bed with and without cavitation. The cavity is taken to be symmetric around the inflection point at x = L/2, and has a length 2λ. (From Schweizer, J., and A. Iken, *J. Glaciol.,* 38, 77–92, 1992. Reprinted from the *Journal of Glaciology* with permission of the International Glaciological Society and the authors.)

fluctuations generated by the flow over the obstacle. In most sliding theories, this is the only contribution to basal resistance.

Form drag may be important where bridging effects occur, that is, where the weight of an ice column is not supported from directly below and the vertical resistive stress, R_{zz}, is nonzero. To calculate the magnitude of the form drag, a simplified basal topography is considered, namely a sinusoidal bed (Figure 7.3)

$$b(x) = B_o \sin\left(\frac{2\pi x}{L}\right). \tag{7.14}$$

If no separation occurs, the vertical resistive stress at the bed is taken to be out of phase with the bed topography in such a way that the pressure on the bed is largest on the stoss side of the obstacle and reaches a minimum on the lee side (Figure 7.3; Lliboutry, 1968). Then

$$R_{zz}(x) = R_o + \Delta R \cos\left(\frac{2\pi x}{L}\right). \tag{7.15}$$

In this expression and in the following, stresses are referred to their value at the glacier sole.

Averaged over one wavelength, the weight of the ice must be supported by the bed, and hence

$$\int_0^L R_{zz}(x)\, dx = 0, \tag{7.16}$$

from which it follows immediately that R_o must be zero. Furthermore, if the bed is perfectly lubricated, skin friction is zero. Then, if τ_b represents the average basal resistance, equation (7.13) for basal drag gives

$$\tau_b = -\frac{1}{L}\int_0^L R_{zz}(x)\,\frac{\partial b}{\partial x}\,dx, \tag{7.17}$$

or

$$\Delta R = -\frac{\tau_b L}{B_o \pi}. \tag{7.18}$$

Note that the vertical coordinate axis is taken positive upward, so that a negative value of R_{zz} corresponds to a pressure larger than lithostatic on the underlying bed. The pressure on the bed is equal to minus the full vertical normal stress in the ice, or

$$P_n = P_o + \frac{\tau_b L}{B_o \pi}\cos\left(\frac{2\pi x}{L}\right). \tag{7.19}$$

Here $P_o = \rho g H$ represents the lithostatic pressure. The minimum pressure on the bed occurs at $x = L/2$ (the inflection point on the lee side of the obstacle; Figure 7.3) and is given by

$$P_m = P_o - \frac{\tau_b L}{B_o \pi}. \tag{7.20}$$

Where the subglacial water pressure equals this minimum pressure, separation of the ice from the bed will occur.

Equation (7.20) relates basal drag to the basal pressure and reflects the assumption that basal resistance arises from compressive stresses acting on the upstream slopes of bed obstacles. As pointed out by Iken (1981), the consequence of this model is that an upper limit to basal drag exists. The minimum pressure cannot become less than the water pressure in the cavities without introducing nonzero acceleration terms in the force-balance equations, and

$$P_m \geq P_w. \tag{7.21}$$

Then, from equation (7.20),

$$P_o - \frac{\tau_b L}{B_o \pi} \geq P_w, \tag{7.22}$$

or

$$\frac{\tau_b L}{B_o \pi} \leq N, \tag{7.23}$$

where $N = P_o - P_w$ represents the effective basal pressure. The upper bound on basal drag depends on the geometry of the bed through the amplitude, B_o, and wavelength, L, of the bed perturbations. This result is derived here for a simple sinusoidal bed, but the analysis by Schoof (2005) shows that an upper bound on basal drag exists for any arbitrary bed geometry and this upper bound depends on bed obstacles that have the steepest slopes. In essence, this upper bound exists because when cavitation occurs, it becomes more difficult to exert sufficient stress on the remaining undrowned bed obstacles (Schoof, 2005).

Although Iken (1981) noted the existence of an upper bound to basal drag where cavitation occurs or, equivalently, a critical water pressure above which sliding was said to become unstable, that study considered only the stable sliding regime with basal drag smaller than the upper bound. Fowler (1987a) argued that for real glaciers basal drag does not reach a maximum because there will always be bed obstacles large enough to offer sufficient form drag to allow basal drag to increase. However, as equation (7.23) shows, as well as the analysis of Schoof (2005), this is true only if the slope of the larger obstacles is greater than that of the obstacles that already have been drowned or cavitated.

The existence of an upper bound for basal drag has important consequences for modeling glacier flow. First, where the driving stress is larger than the maximum basal drag, other resistive stresses must balance part of the driving stress. Most ice-flow models are based on the lamellar flow assumption in which the driving stress is balanced entirely by drag at the glacier bed (Section 4.2), but this may not be appropriate for outlet glaciers approaching flotation ($N \rightarrow 0$). Second, it forces a different view of what constitutes a sliding law. The common view is that such a law relates the sliding velocity to basal drag and effective basal pressure. It is more appropriate to view a sliding relation as expressing basal drag as a function of sliding speed and effective basal pressure (Schoof, 2005).

Lliboutry has suggested a number of relations to link the sliding velocity to the stress distribution calculated above. For example, the velocity can be estimated by comparing the rate of basal melting to the rate of closure of the cavity or by considering the two components of velocity (in the horizontal and vertical directions) and requiring that the net velocity be directed along the lower surface of the ice. For an undulating random bumpy profile with extensive cavitation, Lliboutry (1987a) suggests the following local relation between basal drag and sliding velocity

$$\tau_b = fN + \frac{DU_s}{(fN)^{n-1}}. \tag{7.24}$$

Here f represents a constant that depends on the distribution of obstacle heights; D is a constant that includes the rate factor of the ice, bed roughness, and other parameters; n represents the exponent in Glen's flow law; and N represents the effective subglacial water pressure. The first term on the right-hand side represents Coulomb friction between solids, assumed to be negligible in most sliding theories.

The most common sliding relation used in numerical models is a generalization of the second term on the right-hand side of equation (7.24), and this is often referred to as modified Weertman sliding

$$\tau_b = B_s U_s^p N^q, \tag{7.25}$$

where B_s, P, and q are positive sliding parameters and U_s represents the sliding velocity (for example, Budd et al., 1979; Bindschadler, 1983; Fowler, 1987a). In the more common glaciological notation, this relation is written as

$$U_s = A_s \frac{\tau_b^m}{N^p}. \tag{7.26}$$

Bindschadler (1983) compared various sliding relations against observations and found a best fit for m = 3 and p = 1. In their model of the West Antarctic Ice Sheet, Budd and others (1984) adopted this sliding relation with m = 1 and p = 2.

Sliding relations of the form (7.25) do not allow for an upper limit to basal drag, irrespective of the value of the effective basal pressure. For this reason, Schoof (2005) suggested the following heuristic sliding law:

$$\frac{\tau_b}{N} = C\left(\frac{U_s}{U_s + D_o N^n}\right), \tag{7.27}$$

where D_o is a constant that depends on the wavelength of dominant obstacles, their slope, and the rate factor for glacier ice. Support for a sliding relation of this form comes from finite-element modeling of ice flow past bedrock obstacles (Gagliardini et al., 2007). Their modeling results suggest a sliding law of the form

$$\frac{\tau_b}{N} = C\left(\frac{\chi}{1 + \alpha\chi^q}\right)^{1/n}, \tag{7.28}$$

where

$$\chi = \frac{U_s}{C^n N^n A_s}, \tag{7.29}$$

and

$$\alpha = \frac{(q-1)^{q-1}}{q^q}. \tag{7.30}$$

In these expressions, C is the maximum value reached by τ_b/N (similar to equation (7.23)), and A_s the sliding parameter in the absence of cavitation. Figure 7.4 shows this sliding law for different values of the exponent q. The value of q controls the post-peak

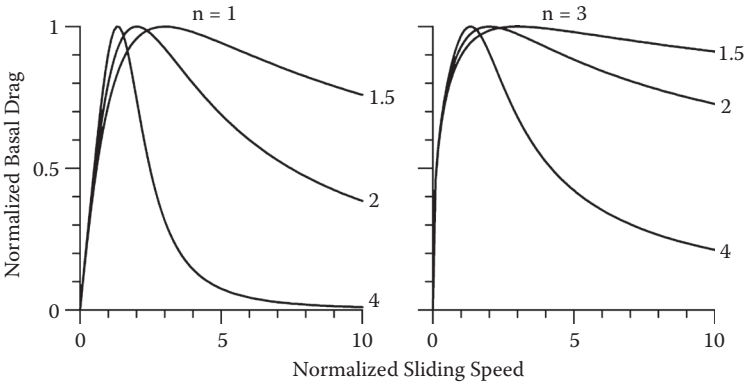

FIGURE 7.4 Normalized basal drag as a function of normalized sliding speed according to equation (7.28) for different values of the exponent, q (indicated by the labels), and for n = 1 (left panel) and n = 3 (right panel).

decrease in basal drag: the larger this exponent, the more rapidly basal drag decreases after peaking. The maximum basal drag corresponds to the sliding velocity

$$U_s = \frac{q}{q-1} A_s C^n N^n. \tag{7.31}$$

(Gagliardini et al., 2007).

Potentially, the double-valued sliding (7.28) can lead to flow instability. In the initial stages of cavitation and sliding, enough bed obstacles remain to provide resistance to flow. As cavitation progresses, and more smaller obstacles are drowned, basal resistance has to come from form drag offered by the remaining obstacles with ice contact. However, the maximum drag able to be generated from these obstacles depends on their slope; thus, unless larger obstacles also have steeper slopes, associated form drag will reach a maximum, irrespective of whether undrowned bed irregularities remain. Should further cavitation occur, basal drag will decrease while the sliding speed continues to increase.

Whether basal drag will reach the upper bound depends on the value of C in equation (7.28) and the effective basal pressure, N. For a sinusoidal bed, Gagliardini et al. (2007) found $C \approx 0.84(2\pi B_o/L) = 1.68\pi R$, where R represents the bed roughness. As derived in Section 7.4, the maximum effective basal pressure is given by the height above buoyancy, H_b (thickness of the ice in excess of the flotation thickness), corresponding to the situation where an easy connection exists between the subglacial drainage system and the proglacial water body. Under those conditions

$$\begin{aligned} \tau_b(\max) &= CN(\max) = \\ &= 1.68\pi R \rho g H_b = \\ &\approx 47 R H_b, \end{aligned} \tag{7.32}$$

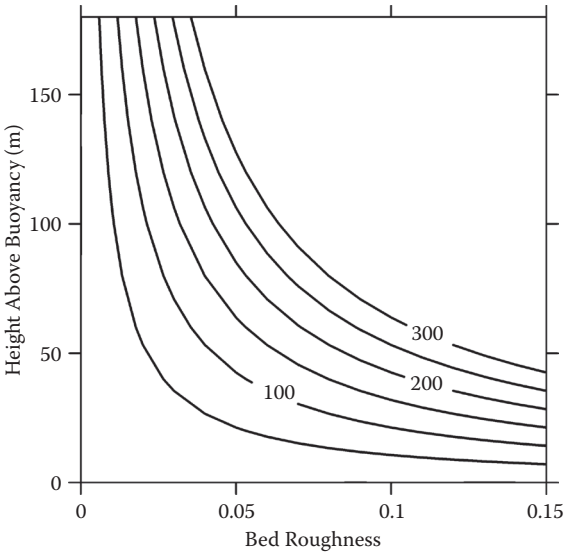

FIGURE 7.5 Contours of maximum basal drag (interval: 50 kPa) as a function of bed roughness and height above buoyancy. Contours for values greater than 300 kPa are not shown.

with basal drag in kPa. Figure 7.5 shows how this upper limit depends on bed roughness and height above buoyancy. For comparatively smooth beds or for glaciers that are close to flotation, the upper limit to basal drag can become less than 100 kPa, making it conceivable that ice flow enters the regime of rapid sliding with decreasing basal resistance.

All these theories contain some degree of simplification and may not be entirely realistic. Perhaps the most important objection is that the bed is assumed to be perfectly lubricated. That is, the tangential shear stress, or skin friction (equation (7.11)), is neglected and all basal resistance is attributed to the form drag resulting from the pressure fluctuations induced by the obstacle. Only in the very special case of clean basal ice may this be an appropriate simplification. In most cases, glaciers do not move frictionless over their bed, as can be inferred from erosive patterns such as glacial grooves and striae in regions formerly overlain by glaciers. Also, where observed, basal ice usually contains debris. As this dirty ice slides over its bed, friction may be expected. Thus, perhaps a more realistic approach is to include the effect of skin friction and to attempt to derive a relation between the sliding velocity and the skin friction (Morland, 1976; Schweizer and Iken, 1992).

The total basal drag, τ_b, is written as the sum of form drag, τ_f (the second term on the right-hand side of equation (7.13)) and tangential skin friction, τ_f, and

$$\tau_b = \tau_t + \tau_f. \tag{7.33}$$

Schweizer and Iken (1992) propose that the sliding velocity must be proportional to the *n*th power of the form drag, τ_f (which they term the "resultant effective shear

stress"), while Morland (1976) considers a sliding relation that links the velocity to the skin friction, τ_t. These approaches probably represent the two limiting cases of form drag being most important and skin friction being dominant. Thus, a general sliding relation may look as follows:

$$U_s \propto C_1\tau_f^p + C_2\tau_t^q, \tag{7.34}$$

where C_1 and C_2 are constants that may depend on the effective water pressure, and other factors as well.

An entirely different approach to the problem of sliding with friction is taken by Boulton (1974), Hallet (1981), and Shoemaker (1986), among others. In these studies, the contact forces between debris particles in the ice and the underlying bed are calculated explicitly. Because this resistive force can be related to both the basal resistance and the velocity of the debris (and hence the velocity of the basal ice), a sliding relation can be derived. For example, Hallet (1981) suggests the following relation:

$$U_s = \frac{\tau_b}{\eta(R + \Omega\mu C_o)}, \tag{7.35}$$

where η represents the viscosity of the basal ice, R is a bed-roughness factor, Ω is a viscous drag term, μ describes the friction between the basal debris and the bed, and C_o denotes the concentration of debris in the basal ice layers. Most of these parameters are ill-constrained, thus limiting the practical use of this relation or variations on it.

7.3 GLACIER FLOW OVER A SOFT BED

In the models discussed so far in this chapter, the bed underneath the ice is taken to be hard and nondeformable. However, large areas previously covered by continental ice sheets are overlain with till, "the ubiquitous glacial deposit by which every former glacier is most surely traced" (Goldthwait, 1971, p. 3). Glacial geologists have long suggested that such sediments under glaciers may be actively deforming as a consequence of forces exerted by the moving ice. As early as 1894, W. J. McGee, in summarizing his work based on field observations in "the magnificent field of the southern Sierra" noted that "if a continuous sheet of comminuted debris intervene, the movement may be divided between its upper and lower surfaces; and if the intercalated sheet be thick, several planes of slip may exist within it and its own motion becomes differential" (McGee, 1894, p. 352). Where subglacial sediments are actively deforming, some fraction of the measured ice velocity will be due to the rate at which the sediment is deforming. Yet, the glaciological community was slow to realize the importance of ice moving over soft beds and potential implications for ice-sheet stability. For example, the 1981 second edition of Paterson's classic *The Physics of Glaciers* does not mention deformable beds. By the time the third edition was published in 1994, an entire chapter was devoted to "Deformation of Subglacial Till." What brought about this "paradigm shift in glaciology" (Boulton, 1986) was the discovery of a meters-thick layer of deforming sediments under Whillans Ice Stream

in West Antarctica in the first half of the 1980s by scientists from the University of Wisconsin, Madison (Blankenship et al., 1986). Prior to this discovery, Geoffrey Boulton and colleagues had been trying to raise the awareness of the glaciological community to the potential importance of soft beds to glacier flow, primarily based on work conducted on Breidamerkurjökull in Iceland, but the observations on Whillans Ice Stream made the community realize the potential scale on which deforming sediments could act and, perhaps, affect the stability of large ice sheets.

Boulton and Jones (1979) pointed out that many glaciers rest on soft beds that consist of sediments that may be deforming. Regions that were formerly ice covered reveal a subglacially deposited till or other unlithified sediment, which appears to be very soft and with a high water content. Boulton and Jones (1979) proposed that if high water pressures develop in the sediments (due to basal melting and low transmissibility of the bed), the effective pressure may be sufficiently low to cause deformation of the subglacial sediments. In fact, Boulton and Hindmarsh (1987) argued that measurements of deformation within the till underlying Breidamerkurjökull in Iceland suggest that 88% of the ice movement is due to such deformation, compared with 12% by sliding at the glacier-bed interface. Similarly, the discovery of a layer of till under Whillans Ice Stream in West Antarctica (Blankenship et al., 1986, 1987) has led Alley and co-workers to advance the hypothesis that the high speeds measured on this ice stream, as well as the very small basal resistance (less than 20 kPa), are the result of the presence of a continuous layer of actively deforming till (Alley et al., 1986, 1987a).

Despite numerous research efforts over the last few decades, understanding of the role of subglacial sediments in modulating glacier flow remains frustratingly limited. How these sediments deform has been a contested topic in glaciology, and different constitutive relations have been proposed and incorporated into numerical ice flow models (c.f. Clarke, 2005). Even the more basic question concerning the extent of deforming sediments appears to be under debate (Boulton et al., 2001; Piotrowsky et al., 2001, 2002). In part, this may be due to the many faces of glacial till and its composition and the difficulties in firmly establishing origins of sediments left behind by glaciers. For example, Piotrowsky et al. (2002, p. 174) note that "the Norfolk Drift is as controversial as it is well known," with various researchers having proposed different origins of this sedimentary deposit. Moreover, the inaccessibility of sediments under glaciers effectively prevents controlled deformation experiments, and most flow laws for till are based on laboratory experiments. In the few experiments where subglacial sediments were accessed directly, observations suggest that till deformation may vary considerably on time scales from hours to days (for example, Kavanaugh and Clarke, 2006).

This section briefly discusses the most common models for till deformation in use by the glaciological community. It falls outside the scope of this book to discuss all relevant observations and theories. Indeed, this is a task better left to scientists with greater expertise in this area.

Boulton and Hindmarsh (1987) describe results of deformation experiments conducted under the margin of Breidamerkurjökull, a major outlet glacier of Vatnajökull in Iceland. Because this represents one of the few in situ measurements of till deformation, it is worthwhile to discuss these observations in some detail. During a series

of experiments, tunnels were excavated within the basal ice and perpendicular to the margin (approximately in the direction of ice flow). Strain markers and piezometers were inserted into the subglacial sediment by drilling small holes, which were plugged after the markers and piezometers were in place. At the end of the experiment (136 to 244 hours), the sediment was excavated and the location of the strain markers noted. The markers buried in the till showed clear signs of shearing motion within the sediment. Boulton and Hindmarsh (1987) therefore conclude that the shear stress exerted by the ice on the sediment causes the sediment to deform, and this deformation is the major contributor to the ice velocity.

From a series of experiments conducted from 1977 to 1983, Boulton and Hindmarsh (1987) obtained seven triplets of values for strain rate in the subglacial till, basal drag, and effective normal pressure, and fitted two rheological models to these data. The first model represents a nonlinear Bingham fluid with yield strength τ_y. Deformation in such a material is zero if the shear stress exerted on it is smaller than the yield strength, while a larger shear stress, τ, results in deformation according to

$$\dot{\varepsilon} = C\frac{(\tau - \tau_y)^p}{N^q}. \tag{7.36}$$

The yield strength is determined by the Mohr–Coulomb failure criterion (for example, Vyalov, 1986, p. 101)

$$\tau_y = C_o + N\tan\phi, \tag{7.37}$$

with C_o the cohesion and ϕ the friction angle, both material properties of the till that may depend on porosity, water content, and other factors. The other model tested by Boulton and Hindmarsh (1987) is the nonlinear viscous fluid model, described by the following rheological relation:

$$\dot{\varepsilon} = D\frac{\tau^s}{N^t}. \tag{7.38}$$

Both rheological models fit the data equally well, and Boulton and Hindmarsh find only a slight rheological nonlinearity ($p = 1.3$, $q = 1.8$ in equation (7.36); $s = 0.6$, $t = 1.2$ in equation (7.38)). Given the paucity of data and the number of adjustable parameters, the model fitting should be viewed with skepticism. More importantly, the drag exerted by the moving ice on the underlying till is calculated from the glacier geometry. In itself, this is a dubious procedure, especially near the glacier terminus, where longitudinal stress gradients can be expected to be important; but moreover, no accurate surface elevation measurements appear to be available for this glacier. Basal drag varying between about 20 kPa and 105 kPa over short distances and time spans (as claimed by Boulton and Hindmarsh, 1987, Figure 7) appears highly improbable if these values are estimated from the driving stress (see also the discussion in Murray, 1997).

TABLE 7.1
Value of the Effective Viscosity for Various Materials

Material	Log (viscosity) in Pa s
Air [(1)]	–4.7
Water [(1)]	–2.9
Olive oil [(1)]	–1.0
Mud flow [(2)]	2.7
Soft clay [(3)]	9–10
Firm clay [(3)]	11–12
Stiff clay [(3)]	13–14
Hard clay [(3)]	14–16
Ice	13–14

Source: Data from (1) Turcotte, D. L., and G. Schubert, *Geodynamics* (2nd ed.), Cambridge, Cambridge University Press, 2002, p. 228; (2) Johnson, A. M., *Physical Processes in Geology*, San Francisco, Freeman, Cooper, & Co., 1970, p. 513; (3) Vyalov, S. S., *Rheological Fundamentals of Soil Mechanics*, Amsterdam, Elsevier, 1986, pp. 120–121.

In most coupled ice-flow/till-deformation models, a linear rheology for the subglacial till is adopted (for example, Alley et al., 1987b; Alley 1989b; MacAyeal, 1989). That is,

$$\tau = \eta \dot{\varepsilon}, \tag{7.39}$$

where the (effective) viscosity, η, may be dependent on the ambient effective pressure. Using the data from Boulton and Hindmarsh (1987), the viscosity of the till under Breidamerkurjökull ranges from $6.5 \cdot 10^{10}$ to $5.6 \cdot 10^{11}$ Pa s. For comparison, Table 7.1 lists viscosities of some other materials.

An entirely different rheological model for water-saturated till is suggested by Kamb (1991), based on experiments conducted on subglacial material recovered from the base of Whillans Ice Stream in West Antarctica. This fast-flowing ice stream is believed to be underlain by a meters-thick subglacial layer that is highly porous and saturated with water at high pore pressure, as suggested by seismic reflection studies (Blankenship et al., 1986, 1987). Subsequent drilling to the bed has confirmed these early inferences (Engelhardt et al., 1990). Samples of till recovered show a highly plastic but cohesive, sticky mud that contains an abundance of rock fragments of pebble size and smaller. Direct-shear tests on the freshly cored till suggest that the till behaves very much like a Coulomb-plastic material with a yield stress of about 2 kPa (Kamb, 1991). In terms of the nonlinear viscous rheology (equation (7.38)), this corresponds to a very large value of the exponent (s ~ 100; Kamb, 1991). Equivalently, perfect plasticity corresponds to a linear rheology (equation (7.39)), but with a very small viscosity, for shear stresses that are larger than the yield stress.

In numerical models, introducing a yield criterion with strain rate switching from zero to some large number when the yield stress is reached is likely to lead

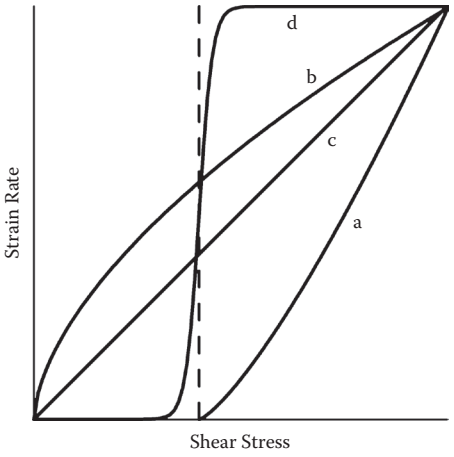

FIGURE 7.6 Relation between strain rate and applied shear stress for four rheological models for subglacial till. Curve a: equation (7.36) with p = 1.3; curve b: equation (7.38) with s = 0.6; curve c: equation (7.39); curve d: equation (7.40). The vertical dashed line indicates the yield strength. Scales are arbitrary.

to numerical instabilities or other problems. To avoid such numerical artifacts, Kavanaugh and Clarke (2006) propose the following relation to describe the rheological behavior of Coulomb-plastic till:

$$\dot{\varepsilon} = \frac{\dot{\varepsilon}_o}{2}\left[1 + \tanh\left(2\pi\frac{\tau-\tau_y}{\Delta\tau}\right)\right]. \tag{7.40}$$

By assigning a large value to the reference strain rate, $\dot{\varepsilon}_o$, and a small value to the failure range, $\Delta\tau$, this relation closely resembles stepwise behavior with yield strength τ_y.

A comparison of the four proposed flow relations for subglacial till is shown in Figure 7.6. Because Boulton and Hindmarsh (1987) found only small nonlinearity for the two relations tested, these are not significantly different from the linear relation, except, of course, that for relation (7.36) no deformation occurs until the yield strength is reached. Kavanaugh and Clarke (2006) measured simultaneously basal water pressure, pore water pressure, sediment deformation, glacier sliding, and sediment strength beneath Trapridge Glacier in Canada's Yukon Territory and, combined with hydromechanical modeling, tested these four flow laws. They conclude that for the duration of the five-day measurements, modeled instrument responses yield the best qualitative agreement with field measurements if Coulomb-plastic rheology is adopted. Iverson and Iverson (2001) use a numerical model to illustrate how deformation profiles such as those measured in the Breidamerkurjökull sediments can result from brief episodes of failure during which the stress locally at some depth exceeds the yield strength of the till at depth, instigating motion of a thin layer of sediment at that depth.

The perfect-plastic model and the (almost) linear-rheological model have important but very different consequences for the flow (and stability) of the overlying glacier. According to the first (Kamb) model, the shear stress on the subglacial layer is limited to the yield strength of the till, and if the till is moving, its flow is presumably driven by horizontal gradients in pressure. Also, in this model, basal drag experienced by the glacier must be small, a few kPa at most. Interpretation of measured surface velocities on Whillans Ice Stream suggest that, indeed, this may the case (Whillans and Van der Veen, 1997). If, on the other hand, the till obeys a linear rheology, as advocated by Alley and co-workers, the speed of the glacier is determined entirely by the viscous properties of the till. Equating the shear stress on the subglacial layer with basal drag, integration of expression (7.39) twice with respect to the vertical coordinate gives the velocity at the top of the till layer (and thus the velocity of the glacier):

$$U_t = \frac{2}{\eta} H_t \tau_b, \tag{7.41}$$

where H_t represents the thickness of the till layer and the velocity at the bottom of this layer is taken to be zero.

The controlling parameter that determines which of these two models applies is the effective viscosity of the subglacial till. To explore this issue somewhat further, consider the flow of a viscous material between two plates. The forces acting on a small element are shown in Figure 7.7. Assuming accelerations are negligible, the sum

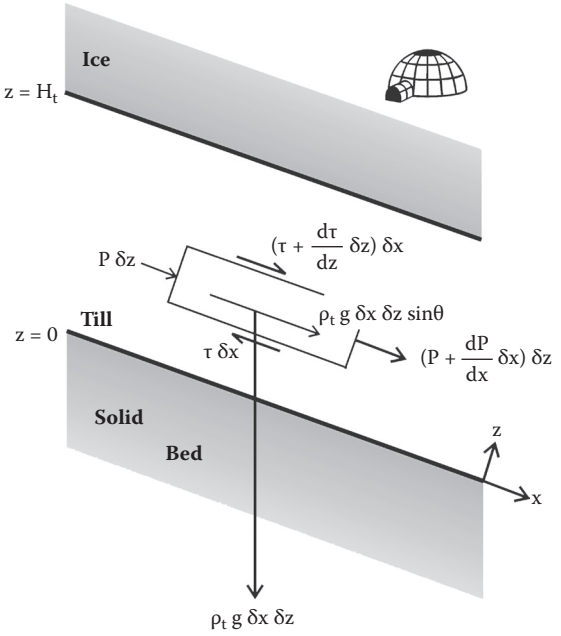

FIGURE 7.7 Forces acting on a small element (δx by δz, and unit width) of deformable material embedded between the glacier sole and a nondeforming solid bed.

of the forces acting in the direction of flow must be zero. Making this sum, and dividing by the volume of the element, gives the balance equation (compare Section 3.1),

$$\frac{\partial \tau}{\partial z} = \frac{\partial P}{\partial x} - \rho_t g \sin\theta, \tag{7.42}$$

where P represents the pressure and θ the slope of the lower boundary (taken positive when the bed slopes downward in the direction of flow, as shown in Figure 7.7). Adopting the linear-viscous model (equation (7.39)), the vertical shear in velocity is linked to the shear stress as

$$\frac{\partial u}{\partial z} = \frac{2}{\eta}\tau. \tag{7.43}$$

Combining equations (7.42) and (7.43) yields

$$\frac{\partial^2 u}{\partial z^2} = \frac{2}{\eta}\frac{\partial P}{\partial x} - \frac{2\rho_t g}{\eta}\sin\theta. \tag{7.44}$$

Integrating this expression twice with respect to the vertical z-coordinate gives the velocity profile in the viscous layer:

$$u(z) = \frac{1}{\eta}\frac{\partial P}{\partial z}z^2 - \frac{\rho_t g}{\eta}\sin\theta\, z^2 + A z + B. \tag{7.45}$$

The two integration constants, A and B, can be determined from the boundary conditions. At the lower boundary of the layer (z = 0), the velocity must be zero, and thus B = 0. Denoting the thickness of the layer by H_t and the velocity at the upper boundary by U_t, the second integration constant is

$$A = \frac{U_t}{H_t} - \frac{H_t}{\eta}\frac{\partial P}{\partial x} + \frac{\rho_t g H_t^2}{\eta}\sin\theta. \tag{7.46}$$

The velocity profile now becomes

$$u(s) = \frac{H_t^2}{\eta}\frac{\partial P}{\partial x}(s^2 - s) - \frac{\rho_t g H_t^2}{\eta}\sin\theta\,(s^2 - s) + U_t s, \tag{7.47}$$

where $s = z/H_t$ denotes a dimensionless vertical coordinate.

From the expression for the velocity profile and using equation (7.43), the shear stress at the top of the viscous layer, and thus the basal drag on the glacier, is found to be

$$\tau_b = \frac{1}{2}\frac{\partial P}{\partial x}H_t - \frac{1}{2}\rho_t g H_t \sin\theta + \frac{\eta}{2}\frac{U_t}{H_t}. \tag{7.48}$$

For very small values of the effective viscosity, η, the third term on the right-hand side may be neglected, and basal drag is determined by the gradient in subglacial pressure and slope of the bed. According to the Alley model, on the other hand, the first two terms are negligible and basal drag is controlled entirely by the viscosity of the till.

To quantify this analysis, consider again the experiments on Breidamerkurjökull, described in Boulton and Hindmarsh (1987). The ambient pressure gradient may, in first approximation, be set equal to the gradient in the ice overburden pressure (thus, gradients in the water pressure are neglected). Then

$$\frac{\partial P}{\partial x} \approx \rho g \frac{\partial H}{\partial x}, \tag{7.49}$$

where H represents the ice thickness. From Figure 1 in Boulton and Hindmarsh (1987) it may be concluded that the bed is near horizontal ($\theta = 0$) and the thickness gradient is equal to the surface slope (about –0.4). The thickness of the till layer is about 0.5 m, so that the contribution to basal drag from the pressure-gradient term (the first term on the right-hand side of equation (7.48)) is about –0.9 kPa. Note that this contribution to the basal drag is negative. This is because the viscous flowing material exerts a drag on the upper plate (i.e., the glacier sole) that is directed along the positive x-axis (the direction of flow). Basal drag on the glacier is taken positive when resisting the flow of the ice and directed along the negative x-axis. In principle, if the third term in equation (7.48) were zero and the bed horizontal or sloping downward in the direction of flow, basal drag on the glacier could thus be negative, with the ice being dragged along by the subglacial till driven by the horizontal pressure gradient. However, for realistic values of the pressure gradient and basal slope, the effect is small, a few kPa at most. The second term on the right-hand side of equation (7.48) is zero (no bed slope), while the third term can be calculated for different values of the effective viscosity. The results of a calculation using $U_t = 23$ m/yr (Boulton and Hindmarsh, 1987) are shown in Figure 7.8. The transition from pressure-driven flow to shearing flow occurs over a relatively narrow range of values of the effective viscosity, namely, about a factor of 10. Given the uncertainty in viscosity (c.f. Table 7.1), it thus seems possible that the till near the margin of Breidamerkurjökull is being squeezed out from underneath the glacier (as illustrated in Figure 7.9), rather than deforming under an applied shear stress.

The "squeezing" hypothesis was proposed by Price (1970) to explain the pattern of moraine ridges observed near the margin of the retreating Fjallsjökull, another glacier in Iceland. The former frontal position is clearly marked by moraine ridges, about 5 to 10 m high. Inside these larger moraines are series of smaller moraine ridges (about 1 to 4 m high) that appear to have formed proglacially, rather than being deposited in a subglacial cavity to be exposed by the retreating ice front. Also, the ridges follow the shape of the ice front, but no evidence appears that the glacier front acts as a bulldozer, building the moraine

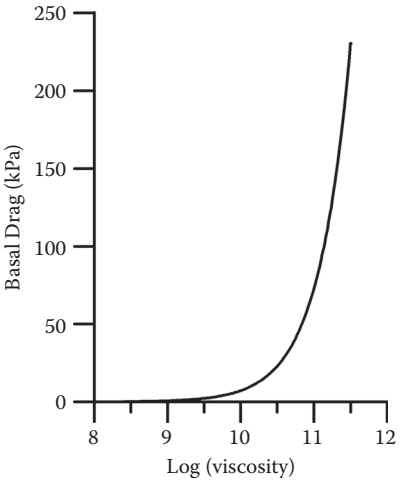

FIGURE 7.8 Basal drag on a glacier resting on a layer of deformable till, as a function of the effective viscosity of the till, calculated from equation (7.48), using $\partial P/\partial x = -4\mu Pa/m$, $H_t = 0.5$ m, $U_t = 23$ m/yr, and assuming zero bed slope.

ridges by plowing up the proglacial deposits. Price (1970) suggests that pressure-driven flow may be triggered by spring meltwater reaching the base of the glacier. The increased water content of the subglacial till would lower the bearing capacity of the till, until the semiliquid water-soaked material is being squeezed out from underneath the glacier.

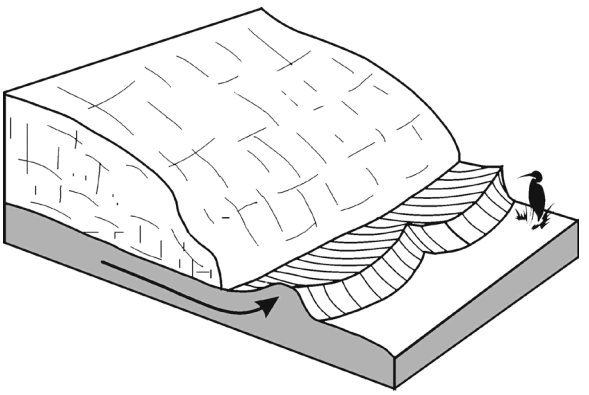

FIGURE 7.9 Illustration of the squeezing of till from underneath the glacier margin to produce proglacial moraine ridges. (From Price, R. J., *Arctic Alpine Res.,* 2, 27–42, 1970. Reproduced by permission of the Regents of the University of Colorado from *Arctic and Alpine Research*.)

7.4 SUBGLACIAL HYDRAULICS

The nature and efficiency of the subglacial drainage system is one of the primary controls on glacier sliding and deformation of subglacial sediments. Where drainage of meltwater is tortuous or impeded, one may expect high water pressures to build up, reducing the effective pressure at the glacier bed, resulting in increased basal sliding speeds (equation (7.26)) or reduced basal friction (equation (7.24)). Similarly, rheological properties of subglacial till depend strongly on the water content, and deformation occurs only when the till is water saturated. Consequently, any model aiming to predict how glaciers and ice sheets evolve over time must include a calculation that describes how the effective basal pressure changes in accordance with the glacier. This, in turn, requires a model for how meltwater at the glacier bed is routed underneath the glacier.

In 1972, Hans Weertman published a paper entitled, "General Theory of Water Flow at the Base of a Glacier or Ice Sheet," which started with the following comment: "There is at present no reasonably complete theory of the flow of water beneath glaciers and ice sheets. The theories that have been developed describe only limited parts of the problem" (Weertman, 1972, p. 287). Sad to say that 40 years later, this statement is perhaps even more true than when originally written. At the time, models for water flow at the bed consisted of sheet flow with variable thickness, and concentrated drainage through a system of tunnels either incised into the ice or into the bedrock underneath. Since then, the subglacial landscape has become even more muddied with the introduction of drainage through a linked-cavity system and the realization that many glaciers and ice sheets may be resting on soft sediments. As a result, despite a large number of theoretical analyses and increasingly more in situ observations, a general theory remains elusive. What is fairly certain from observations is that different drainage systems exist under different glaciers and, to complicate matters further, that one drainage system can morph into another, depending on supply of meltwater to the glacier bed, with consequences for glacier discharge. It has been suggested that rapid changes in glacier flow (such as surges) are associated with the switch from one drainage system to another (Fowler, 1987b; c.f. Section 10.4). Schoof (2010) proposes that faster flow on Greenland outlet glaciers is driven by variability in the input of water to the bed due to dynamic switching between channelized and linked-cavity drainage systems.

Before discussing the various drainage systems and their implications on glacier flow, it is instructive to first consider the range of possible water pressures underneath a glacier. This range can be determined independent of the water flux or nature of the drainage system and provides modelers with reasonable bounds on the effective basal pressure used in most sliding laws.

The maximum water pressure can be found by considering the effective basal pressure, N, defined as the difference between the weight-induced pressure of the ice above, P_o, and the water pressure, :

$$N = P_o - P_w = \\ = \rho g H - P_w. \tag{7.50}$$

The effective basal pressure cannot become negative, as this would correspond to a net upward force exerted on the base of the ice. Thus, the water pressure cannot become larger than the ice overburden pressure, and

$$P_w^{max} = \rho g H, \tag{7.51}$$

noting that P_w is taken positive when directed upward. If the water pressure equals this maximum value, the entire weight of the ice is carried by the subglacial water and the effective basal pressure is zero.

An expression for the minimum water pressure can be derived from the condition that subglacial water must be able to reach the glacier terminus. The discharge of water is driven by the downslope component of gravity and by the gradient in water pressure. Because the total pressure gradient is negative in the direction of flow, it is convenient to introduce Γ_t, defined as the negative of the total pressure gradient:

$$\Gamma_t = -\left(\rho_w g \frac{\partial b}{\partial x} - \Gamma_w\right), \tag{7.52}$$

where ρ_w denotes the density of (fresh) water, b the basal elevation (negative if below sea level), and Γ_w minus the gradient in water pressure. The first term between the brackets represents the component of gravity driving subglacial water in the basal downslope direction. If the water is to reach the glacier terminus, the expression between brackets must be smaller than zero, so

$$\Gamma_w \geq \rho_w g \frac{\partial b}{\partial x}, \tag{7.53}$$

or

$$\frac{\partial P_w}{\partial x} \leq -\rho_w g \frac{\partial b}{\partial x}. \tag{7.54}$$

Integrating this expression with respect to the flow direction, x, gives the minimum water pressure needed to discharge water toward the terminus,

$$P_w^{min} = -\rho_w g b + C. \tag{7.55}$$

Note that the basal elevation, b, is negative when below sea level, so that in general, the minimum pressure is positive. The integration constant, C, is given by

$$C = g b_{gr} (\rho_w - \rho_s), \tag{7.56}$$

with b_{gr} the basal elevation at the glacier terminus (or the grounding line, if a peripheral ice shelf exists) and ρ_s the density of sea water. This constant takes into account the difference in density of fresh water and of sea water. If C were zero, fresh water

would not be able to flow out from under the glacier and sea water would be injected under the glacier (Lingle and Brown, 1987). However, the value of C is small, and for the present discussion this constant may be neglected.

The minimum water pressure corresponds to the case of a subglacial aquifer with zero impedance or to water flowing in a film underneath the glacier (Weertman, 1972). The effective pressure is then

$$N^{max} = \rho g \left(H + \frac{\rho_w}{\rho} b \right), \tag{7.57}$$

which represents the infamous height above buoyancy, used in many modeling studies (for example, Van der Veen, 1987; Budd and Jenssen, 1987; Nick et al., 2010). This model applies if there is a full and easy water connection to the sea. However, in most cases, water flow may be expected to be obstructed to some extent, and larger water pressures are needed to overcome the resistance of the basal drainage system.

For a glacier resting on soft (perhaps deforming) sediment, the bed may be a water-saturated layer of porous material that acts as an aquifer for the discharge of the subglacial water (Lingle and Brown, 1987). The flow of water is driven by horizontal pressure gradients and described by Darcy's law. Accounting for the slope of the bed (z = b), the gradient in subglacial water pressure is given by (Lingle and Brown, 1987)

$$\frac{dP_w}{dx} = -\rho_w g \frac{db}{dx} - \frac{\rho_w g}{K} U_w, \tag{7.58}$$

where ρ_w denotes the density of the subglacial water, U_w the volume flux of water per unit of aquifer cross-sectional area, and K the hydraulic conductivity of the porous material. The first term on the right-hand side represents the pressure gradient needed to drive water along a sloping bed, and the second term represents the pressure gradient needed to overcome the impedance of the aquifer.

Lingle and Brown (1987) apply the aquifer model to Whillans Ice Stream in West Antarctica. Because the hydraulic conductivity of the subglacial layer is unknown, they adopt a modified Weertman sliding relation (equation (7.26)), so that the effective pressure (and hence the water pressure) can be calculated from the sliding velocity (calculated from mass-balance considerations) and basal drag (which is equated with driving stress). The inferred values for the hydraulic conductivity fall in the range of 0.019 to 0.064 m/s, which is orders of magnitude larger than the maximum hydraulic conductivity of water-saturated till (about $1.6 \cdot 10^{-6}$ m/s; Boulton and Jones, 1979). On the basis of this result, Lingle and Brown (1987) conclude that water flow through an aquifer is not likely to occur under Whillans Ice Stream, because for realistic conductivities, the pressure gradients needed to drive the subglacial water toward the grounding line become unrealistically large. Instead, they suggest that advection of the water and till mixture may be the mechanism responsible for the discharge of subglacial water. Alley (1989a), on the other hand, argues that because water flow through a subglacial aquifer is so ineffective under this ice stream, where

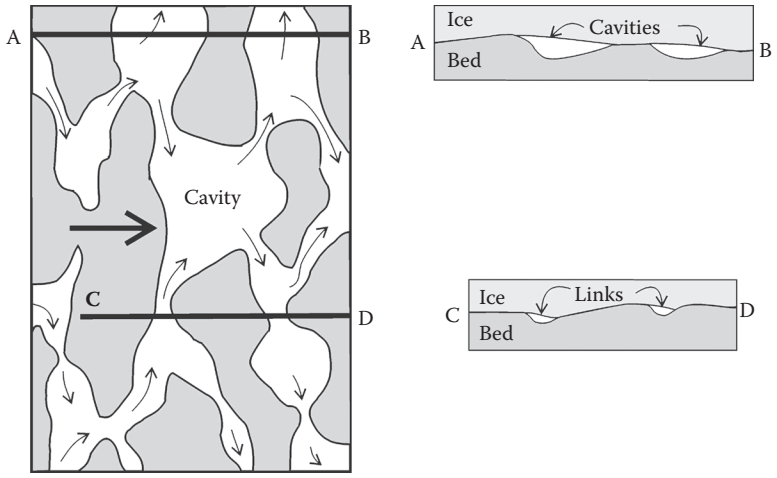

FIGURE 7.10 Schematic illustration of the linked-cavity system. The left panel presents a map view with shading indicating where the ice is in contact with the bed and small arrows showing the direction of water discharge through the network. The panels on the right give the vertical cross-sectional view along the lines AB and CD in the left panel; cavities form on the lee side of large obstacles in the bed, while the connecting links form behind smaller obstacles. (From Kamb, B., *J. Geoph. Res.,* 92(B), 9083–9100, 1987. Copyright by the American Geophysical Society.)

meltwater generation is large, the aquifer may be neglected entirely and water discharge occurs at the interface of basal ice and subglacial till.

A different model for the subglacial hydraulics is the linked-cavity system, schematically shown in Figure 7.10 (Walder, 1986; Fowler, 1987a; Kamb, 1987). As noted in Section 7.2, cavities may form on the lee side of basal obstructions. If there is an ample supply of meltwater, small channels, or links, may form between such cavities, probably on the lee side of lower bumps in the bed. Such a linked-cavity system will be stable if the closure of these links due to flow of ice from upglacier, as well as downward creep of ice from directly above, is compensated for by melting of the roof, due to viscous heat dissipation in the channel. Kamb (1987) argues that, provided the sliding velocity is sufficiently large and the water pressure not too high (but still high), the links will be stable. However, if the sliding velocity decreases or the water pressure increases, the rate of melting becomes too large for the ice flow and creep to keep the roof of the link in place. When this happens, the link may develop into a tunnel, and the glacier may become unstable.

To actually calculate the subglacial pressure in a linked-cavity system, an assumption about the dependency of the sliding velocity of the glacier on the effective pressure is needed and the shape of the conduits linking the cavities needs to be prescribed. The resulting relations are rather complex (Walder, 1986, equation (11); Kamb, 1987, equations (38) and (42)), but all show that the water pressure increases as the interstitial water flux increases. This result is fundamentally different from that derived by Röthlisberger (1972) for water flow through subglacial channels.

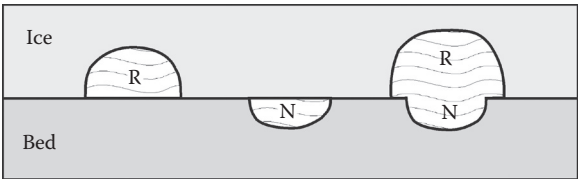

FIGURE 7.11 Cross-sectional view of a Röthlisberger-channel (left), a Nye-channel (middle), and an N-channel overlain by an R-channel (right).

Röthlisberger-channels, or R-channels, are at the base of a glacier and incised upward into the ice, as opposed to Nye-channels, or N-channels, that are incised downward into the glacier bed (Figure 7.11). Röthlisberger (1972) makes the assumptions that the circular conduits are in steady state (that is, melting of the roof is balanced by creep closure under the weight of the ice above), that no heat is transported by the water flowing through the channel, and that the stress in the ice above the channel is isotropic and homogeneous. Under these restrictions, a relation between pressure gradient and water flux can be derived, as shown in Section 7.5. According to the result, the water pressure, P_w, decreases as the discharge increases.

No consensus has been reached among glaciologists as to which model for the subglacial hydraulics is most appropriate. Weertman (1972) argues that channelized drainage is not very likely. A requisite for channelized water flow is that the conduits are able to capture subglacial meltwater that is formed under the entire glacier. For R-channels, and for N-channels that run approximately parallel to the ice-flow direction, the pressure gradient in the vicinity of the conduit is such that it drives water away from the channel rather than into it. Only a tributary N-channel may be able to capture the surrounding meltwater. However, Weertman and Birchfield (1982) doubt whether such channels can exist over extended periods of time. Erosion due to sliding of the glacier is likely to destroy the far ends of the N-channels faster than they can be deepened by the flowing water. Thus, the water flow through the channel decreases, thereby further shortening the conduit. On the other hand, Hooke (1989) argues that observational evidence favors a model in which a linked-cavity system is transected by a few broad, low conduits that drain the meltwater more directly. Most likely, the nature of the subglacial water flow varies from glacier to glacier and possibly throughout the year as well. As noted by Walder (2010), the details about how water is delivered to the main drainage paths (R-channels or linked cavities) may not be crucial and is likely governed by expressions similar to Darcy's law for water flow through porous media (as assumed in Flowers, 2008).

7.5 TUNNEL DRAINAGE

For temperate glaciers, meltwater may form at the surface and enter the glacier through a network of veins, crevasses, and englacial conduits, ultimately collecting at the glacier bed and discharged through the subglacial drainage system. The exact nature of the englacial drainage system remains a subject of debate, in particular how surface meltwater collects in englacial conduits. Irrespective

of the details, it is generally assumed that at some depth below the surface the small veins and drainage tubes have evolved into an arborescent system of englacial tunnels (Shreve, 1972; Röthlisberger and Lang, 1987; Hooke, 1989). This is because the release of potential energy as water flows deeper into the glacier tends to favor the growth of larger veins at the expense of smaller ones (Shreve, 1972; Röthlisberger, 1972).

In many instances it is not very practical to discuss glacier drainage in terms of individual veins and tunnels. Rather, the overall water flow is commonly described in terms of the water pressure potential, defined as (Shreve, 1972; Lawson, 1993)

$$\phi = \phi_o + \rho_w g z + \rho g(h - z) + P(\dot{r}). \tag{7.59}$$

The flow of water is driven by the gradient in ϕ such that the water flows in the direction perpendicular to the surfaces on which the water potential is constant. In equation (7.59), ϕ_o represents a reference potential, taken constant, z the elevation above a horizontal reference surface, and $\dot{r}$ the rate of tunnel closure due to creep of ice. The second term on the right-hand side represents the potential energy of the water, while the third term corresponds to the water pressure, assumed to be equal to the weight of the overlying ice. The last term accounts for the difference between the water pressure in a conduit, and the ice overburden pressure.

Alternatively, retaining the water pressure as a variable, the potential is

$$\phi = \phi_o + \rho_w g z + P_w. \tag{7.60}$$

Applying this expression at the glacier base (z = b) and differentiating with respect to x gives the pressure gradient introduced in equation (7.52):

$$\Gamma_t = -\frac{\partial \phi}{\partial x} = \\ = -\left(\rho_w g \frac{\partial b}{\partial x} + \frac{\partial P_w}{\partial x}\right). \tag{7.61}$$

At this point, it may be useful to define some commonly used hydrological terms (indicated in Figure 7.12). The *piezometric height* is defined as the elevation difference between the level to which water would rise in a borehole connecting the conduit to the free surface (at atmospheric pressure) and the depth at which the conduit is located. Although the conduit may be located anywhere within the glacier, the piezometric height usually refers to the glacier bed. The surface connecting the piezometric elevations at various places in the glacier is called the *piezometric surface* or *hydraulic grade surface*. The piezometric height, H_p, is a direct measure of the water pressure in the conduit, and

$$\rho_w g H_p = P_w. \tag{7.62}$$

The piezometric height is also referred to as *pressure head*. If the height of the piezometric surface is referenced to a horizontal datum surface, the term *hydraulic head*

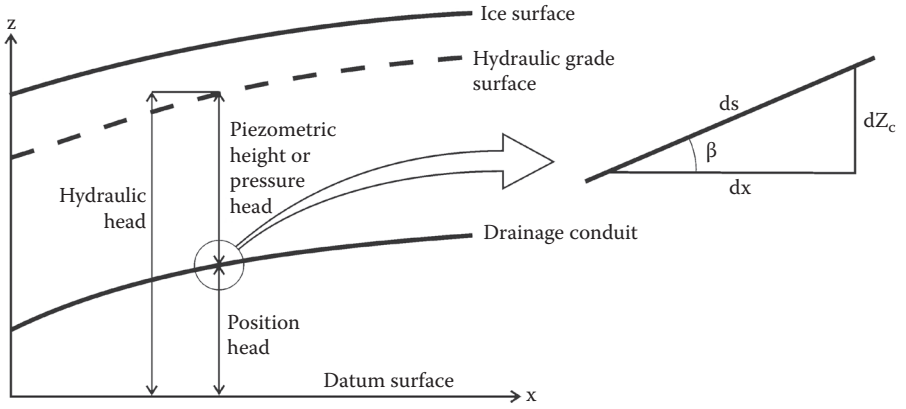

FIGURE 7.12 Definition of hydraulic terms and geometry used in the Röthlisberger model. The pressure head represents the height above the conduit of the piezometric level, that is, the level to which water would rise in a borehole connecting the conduit to the upper ice surface. The surface connecting the piezometric water levels at different points on the glacier is called the hydraulic grade surface. The height of the hydraulic grade surface above a horizontal reference (datum) surface is termed the hydraulic head. The height of the conduit above the datum surface is called the position head. Water flow in the conduit is driven by the slope of the hydraulic grade surface or, equivalently, by the gradient in the hydraulic head.

is used. The hydraulic head is the sum of the pressure head and the height of the conduit above the reference level, called the *position head*. The hydraulic head is equivalent to the water pressure potential.

Theoretical treatment of water flow in or under glaciers usually applies to steady conditions and constant water flux through an idealized tunnel or conduit. The tunnel is assumed to be circular, and its size is determined by the balance between melting of the tunnel walls due to frictional heating from the water passing through and creep closure due to the weight of the ice above. In this section, the model developed by Röthlisberger (1972) for drainage through tunnels is discussed in some more detail to illustrate the complexities involved in formulating a model for subglacial drainage. While this model is usually applied to estimate the water pressure at the glacier bed (for example, Bindschadler, 1983; Greuell, 1992), it may also be used to describe the water flow in englacial tunnels.

The tunnel or conduit is inclined at an angle β with the horizontal x-axis, such that $\tan\beta = dZ_c/dx$, with Z_c the elevation of the tunnel (defined with respect to a horizontal reference level; following the commonly used definition of the vertical z-axis, sea level is chosen as reference level, and $Z_c < 0$ if below sea level). For ease of discussion, the tunnel is assumed to be in the (x, z)-plane, so the length of a tunnel element is given by

$$ds = \frac{dx}{\cos\beta}. \tag{7.63}$$

The flux of water passing through a cross-section of tunnel per unit time is Q, assumed to be known and considered constant at any particular cross-section.

The change in water pressure, dp_w, over a horizontal distance dx can be expressed in terms of the water pressure potential in the tunnel, $\phi_c = \phi(Z_c)$, using equation (7.60) and is

$$\begin{aligned} dP_w &= d\phi_c - \rho_w g\, dZ_c = \\ &= d\phi_c - \rho_w g \tan\beta\, dx. \end{aligned} \tag{7.64}$$

The second term on the right-hand side represents the change in pressure due to the change in potential head. That is, as water flows through an inclined tunnel, it gains or loses potential gravitational energy, depending on whether the tunnel is sloping downward or upward. The first term on the right-hand side of equation (7.64) represents the pressure loss associated with frictional heating.

To estimate the melting rate, it is assumed that the transfer of energy from the water to the surrounding ice occurs instantaneously, so that the heat produced in an element of the tunnel is used to melt the walls of the same element. If changes in the discharge velocity are neglected, the energy produced per unit time in the tunnel element is (Röthlisberger, 1972)

$$dE = Q\, d\phi_c. \tag{7.65}$$

Part of this energy is used to adjust the temperature of the water to the pressure melting temperature, T_p. The change of the pressure melting temperature with water pressure is given by $C_t = -7.4 \cdot 10^{-8}$ K/Pa, so for a change in water pressure equal to dP_w, the change in pressure melting temperature is

$$dT_p = C_t\, dP_w. \tag{7.66}$$

The amount of water that needs to be heated per unit time is Q, so the energy needed to adjust the water temperature is

$$dE_t = -C_t C_w \rho_w Q\, dP_w, \tag{7.67}$$

where $C_w = 4.217 \cdot 10^3$ $Jkg^{-1}K^{-1}$ represents the specific heat capacity of water. The energy available for melting of the conduit walls is found by subtracting this expression from the energy production term (7.65) and is

$$\begin{aligned} dE_m &= dE - dE_t = \\ &= Q\, d\phi_c + C_t C_w \rho_w Q\, dP_w, \end{aligned} \tag{7.68}$$

noting that $C_t < 0$. The volume of ice melted per unit time from the walls of the tunnel element is

$$dV_m = (\rho L_f)^{-1}\, dE_m, \tag{7.69}$$

in which $L_f = 334 \cdot 10^5$ J/kg represents the specific latent heat of fusion and ρ the density of ice.

Under steady-state conditions, the volume of ice melted balances the rate at which the tunnel walls contract due to creep closure. The closure rate is derived in Section 3.6 and is

$$S = \frac{A P_e^n}{(n-1)2^n}, \tag{7.70}$$

in which A represents the rate factor of ice; n the exponent in the flow law; and P_e the effective pressure, that is, the difference between the ice overburden pressure, P_i, and the water pressure, P_w. Except for the constants in the denominator, this expression is the same as that derived by Nye (1953) and used by Röthlisberger (1972). Writing

$$\bar{A} = \frac{A}{(n-1)2^n}, \tag{7.71}$$

the rate at which the radius, r, of the circular tunnel decreases due to creep closure is

$$\frac{dr}{dt} = \bar{A} P_e^n r. \tag{7.72}$$

Thus, for an element of length ds, the change in volume per unit time due to creep closure is

$$\begin{aligned} dV_c &= 2\pi \frac{dr}{dt} ds = \\ &= 2\pi \bar{A} P_e^n r^2 ds. \end{aligned} \tag{7.73}$$

Equilibrium conditions require that creep closure balances melting of the tunnel walls and $dV_m = dV_c$, or

$$2\pi \bar{A} P_e^n r^2 ds = (\rho L_f)^{-1} dE_m. \tag{7.74}$$

The derivation is almost complete now. The energy available for melting is given by equation (7.68) and substitution in equation (7.74) yields the expression from which the water-pressure gradient can be obtained if the radius of the conduit is known.

The size of the tunnel can be eliminated from the above-derived equations by relating the radius, r, to the water flux, Q. If the flow in the tunnel is turbulent, the empirical Manning formula

$$Q = \pi r^2 \frac{R^{2/3}}{m\sqrt{\rho_w g}} \left(\frac{d\phi_c}{ds} \right)^{1/2}, \tag{7.75}$$

can be used to eliminate the tunnel radius (Röthlisberger, 1972). In equation (7.75), m represents the Manning roughness coefficient and R the hydraulic radius, that is, the cross-sectional area divided by the radius. For a circular tunnel, R = r/2. The

Manning roughness coefficient is of the order of 10^{-1} to 10^{-2} $m^{-1/3}$ s, depending on the roughness of the tunnel walls. Rearranging equation (7.75) gives

$$r^{8/3} = \frac{Q\, m\, 2^{2/3} \sqrt{\rho_w\, g}}{\pi} \left(\frac{d\phi_c}{ds} \right)^{-1/2} . \tag{7.76}$$

Instead of the Manning formula (7.75), other expressions relating the water flux to the tunnel size have also been used (c.f. Lawson, 1993). However, whichever relation is used, the procedure remains the same, namely, eliminating the tunnel radius from the equilibrium condition (7.74). While the resulting expression for the pressure gradient may be different, the essential characteristics of the tunnel system appear to be the same as described by the Röthlisberger model.

The final expression is found by combining equations (7.68), (7.74), and (7.76), giving

$$\begin{aligned} \bar{A}\, P_e^n\, \pi^{1/4}\, 2^{3/2}\, m^{3/4}\, Q^{3/4} \left(\rho_w g\right)^{3/8} \rho L_f \left(\frac{d\phi_c}{ds} \right)^{-3/8} ds \; &= \\ = \; Q\, d\phi_c \; + \; C_t\, C_w\, \rho_w\, Q\, dP_w . & \end{aligned} \tag{7.77}$$

Dividing by $ds = dx/\cos\beta$ yields

$$Q \frac{d\phi_c}{dx} \; + \; C_t C_w\, \rho_w\, Q \frac{dP_w}{dx} \; = \; \bar{A}\, D \left(\cos\beta\right)^{-11/8} m^{3/4}\, Q^{3/4}\, P_e^n \left(\frac{d\phi_c}{dx} \right)^{-3/8} , \tag{7.78}$$

with

$$D \; = \; 2^{2/3}\, \pi^{1/4}\, L_f\, \rho (\rho_w g)^{3/8} . \tag{7.79}$$

To apply this expression to find the basal water pressure, the substitution

$$\begin{aligned} \phi_c \; &= \; \phi_b \; = \\ &= \; \phi_o \; + \; \rho_w\, g\, b \; + \; P_w , \end{aligned} \tag{7.80}$$

is made, giving

$$\begin{aligned} \left(\frac{dP_w}{dx} + \rho_w g \tan\beta \right)^{11/8} \; + \; C_t C_w \rho_w \frac{dP_w}{dx} \left(\frac{dP_w}{dx} + \rho_w g \tan\beta \right)^{3/8} \; = \\ = \; \bar{A}\, D (\cos\beta)^{-11/8}\, m^{3/4}\, Q^{-1/4} (\rho g H \; - \; P_w)^n . \end{aligned} \tag{7.81}$$

Obviously, this equation cannot be solved analytically, and the water pressure has to be determined by integrating equation (7.81) numerically. The usual procedure is to start the integration at the glacier terminus, where the water pressure is assumed to be known. If the glacier terminus is grounded on land above sea level, the usual

boundary condition is that the water pressure equals the atmospheric pressure, while for termini grounded below sea level, the water pressure is assumed hydrostatic. However, these conditions may not always apply, and in some instances, water can emerge under pressure at the glacier terminus (Lawson, 1993).

Instead of solving equation (7.81) numerically, an approximate analytical solution can be found by neglecting terms that are small. Fowler (1987a) argues that, in first approximation, the gradient in water pressure may be neglected compared with the term involving the slope of the bed. That is,

$$\frac{dP_w}{dx} << \rho_w g \tan\beta, \tag{7.82}$$

leading to the approximate solution

$$P_w = \rho g H - \left(\frac{(\rho_w g \sin\beta)^{11/8}}{\bar{A} D m^{3/4}} Q^{1/4} \right)^{1/n}. \tag{7.83}$$

According to this solution, the water pressure is constant in a drainage tunnel, and it changes only where tributary tunnels join and the water flux changes. This approximation fails near the glacier terminus, where the water pressure is either hydrostatic or equal to the atmospheric pressure. If the gradient in water pressure were to be zero near the terminus, the water pressure would be equal to the atmospheric or hydrostatic pressure under the whole glacier. In addition, the approximate solution does not apply to tunnels that are horizontal or inclined upward.

Perhaps the most important result of the Röthlisberger model is that the water pressure is inversely related to the discharge flux (as can best seen from inspection of the approximate solution (7.83)). That is, if the discharge increases, the pressure gradient decreases. This is fundamentally different from the linked-cavity system (Kamb, 1987) in which the pressure increases as the water flux becomes larger. The theoretical description of other drainage systems essentially follows the analysis of Röthlisberger (1972), that is, steady-state conditions are adopted, with creep closure of the drainage conduits or cavities being balanced by melting of the ice.

The assumption of steady state may not be entirely realistic. There are important temporal changes in the amount of water added to the drainage system, for example, after a heavy rainfall event. Röthlisberger and Lang (1987) study the effect of changes in water flux with time by repeatedly calculating the steady-state water pressure using equation (7.81). For short-term fluctuations, with periods of a day or so, the size of the conduits cannot adjust rapidly enough, and the water pressure varies in phase with the discharge flux. For annual variations, it may be that the conduits adjust to the varying water input, so that steady-state conditions remain approximately valid. If so, variations in water pressure are out of phase with the water flux, and the seasonal decrease in discharge during the winter months may lead to higher water pressures. This means that the effective basal pressure is smallest during the winter season, resulting in maximum sliding speeds during that time of the year. On the other hand, observations on Columbia Glacier, Alaska, show a seasonal

maximum in spring (May) and a minimum in fall (late September) (Krimmel, 1997). This suggests highest basal water pressures in the spring when water input to the glacier is largest. The high water pressures may be the result of the inability of the drainage system to accommodate increased discharge. Perhaps the drainage tunnels partly collapse during the winter when insufficient meltwater is available for countering creep closure. Starting in the spring and continuing through the summer, the tunnel system develops more fully and becomes more efficient in draining subglacial water. If correct, this model implies that even on a seasonal scale, time evolution of the drainage system must be incorporated into the theory.

Another reservation about the tunnel model is the assumption that the shape of the tunnels is circular. This may be reasonable for englacial tunnels entirely within the ice, but for tunnels at the glacier bed, the circular shape may be unrealistic. However, if the shape of the tunnel is (approximately) semicircular, the derivation presented above should also apply. More important is the question whether the tunnel will be completely filled with water. Paterson (1994) argues that for some distance upstream of the terminus, it is likely that the tunnel is only partially filled, in which case ice will be melted from the sides of the tunnel, but not from its roof. This would result in broad and low drainage tunnels. Given the many other approximations made in the theoretical descriptions, it is doubtful whether such a change has important consequences.